A Unique Role of Carboxylesterase 3 (Ces3) in β-Adrenergic Signaling–Stimulated Thermogenesis

Li Yang,[1] Xin Li,[1] Hui Tang,[2] Zhanguo Gao,[1] Kangling Zhang,[2] and Kai Sun[1,3]

Diabetes 2019;68:1178–1196 | https://doi.org/10.2337/db18-1210

OBESITY STUDIES

Carboxylesterase 3 (Ces3) is a hydrolase with a wide range of activities in liver and adipose tissue. In this study, we identified Ces3 as a major lipid droplet surface-targeting protein in adipose tissue upon cold exposure by liquid chromatography—tandem mass spectrometry. To investigate the function of Ces3 in the β-adrenergic signaling–activated adipocytes, we applied WWL229, a specific Ces3 inhibitor, or genetic inhibition by siRNA to *Ces3* on isoproterenol (ISO)–treated 3T3-L1 and brown adipocyte cells. We found that blockage of Ces3 by WWL229 or siRNA dramatically attenuated the ISO-induced lipolytic effect in the cells. Furthermore, Ces3 inhibition led to impaired mitochondrial function measured by Seahorse. Interestingly, Ces3 inhibition attenuated an ISO-induced thermogenic program in adipocytes by downregulating *Ucp1* and *Pgc1α* genes via peroxisome proliferator–activated receptor γ. We further confirmed the effects of Ces3 inhibition in vivo by showing that the thermogenesis in adipose tissues was significantly attenuated in WWL229-treated or adipose tissue–specific Ces3 heterozygous knockout (Adn-Cre-Ces3$^{flx/wt}$) mice. As a result, the mice exhibited dramatically impaired ability to defend their body temperature in coldness. In conclusion, our study highlights a lipolytic signaling induced by Ces3 as a unique process to regulate thermogenesis in adipose tissue.

Excessive accumulation of triacylglycerol in adipose and other tissues has been linked to obesity and obesity-associated pathology (1,2). Therefore, reducing the lipid burden without increasing the circulating lipid contents may reveal an efficient therapeutic strategy to prevent and combat obesity-related diseases, such as type 2 diabetes and cardiovascular diseases (2). In general, triacylglycerol and other lipid contents are stored in the cytosol lipid droplets (LDs). These LDs are highly dynamic, and hundreds of proteins have been discovered to associate with them (2,3). These proteins function as gatekeepers at the surface of LDs and are tightly regulated by physiological and/or pathological conditions (4,5).

Among the LD surface proteins, lipases such as adipose triglyceride lipase (ATGL) and hormone-sensitive lipase (HSL) play a major role in the degradation of LDs via lipolysis (6,7). These enzymes form an ATGL/HSL axis and function as a cascade for lipolysis in response to energy demands under tight regulation of endocrine pathways (8). The most important regulation of this lipolytic axis is via the β-adrenergic receptor–triggered protein kinase A (PKA) activation pathway (9). Despite this well-known regulation, local events of lipolysis on the surface of LDs by the other participators, especially novel hydrolases, remain largely unknown (10).

Brown adipose tissue (BAT) has been recognized as the predominant energy-burning organ (11). BAT possesses a unique thermogenic protein in its mitochondrial transmembrane domains named UCP1 (12–14). Interestingly, the UCP1-positive beige or brite cells were also identified in subcutaneous white adipose tissue (sWAT) (14,15). Multiple cell stimuli, such as β-adrenergic stimulation, peroxisome proliferator–activated receptor γ (PPARγ) agonist treatment, and vascular endothelial growth factor-A overexpression, may trigger the "browning" of sWAT to generate the beige cells (16–19). Of note, β-adrenergic signaling–triggered lipolysis provides free fatty acids

[1]Center for Metabolic and Degenerative Diseases, Brown Foundation Institute of Molecular Medicine for the Prevention of Human Diseases, University of Texas Health Science Center at Houston, Houston, TX
[2]Pharmacology and Toxicology Department, University of Texas Medical Branch at Galveston, Galveston, TX
[3]Department of Integrative Biology and Pharmacology, Graduate Program in Cell and Regulatory Biology, Graduate School of Biomedical Sciences, University of Texas Health Science Center at Houston, Houston, TX
Corresponding author: Kai Sun, kai.sun@uth.tmc.edu

Received 12 November 2018 and accepted 1 March 2019
This article contains Supplementary Data online at http://diabetes.diabetesjournals.org/lookup/suppl/doi:10.2337/db18-1210/-/DC1.
L.Y. and X.L. contributed equally to this work.

(FFAs) to activate UCP1 in brown and beige adipocytes (20,21). The FFAs serve not only as cofactor and activator but also as the fuel for UCP1 to trigger the nonshivering thermogenesis (22,23). Interestingly, a recent study challenged the role of lipolysis in BAT by showing that Comparative Gene Identification-58 (CGI-58)–dependent lipolysis on the cytosolic LDs is not essential for cold-induced thermogenesis in BAT (24). Instead, the study highlighted the function of lipolysis in WAT on regulating thermogenesis (25,26). The study demonstrated the nonessential role of lipolysis via the classical ATGL/HSL/CGI-58 pathway in BAT. However, it may not rule out the function of lipolysis via other pathways on thermogenesis in this organ.

In this study, we identified carboxylesterase 3 (Ces3) as a unique enzyme on LDs that couples lipolysis and thermogenesis in both sWAT and BAT. Ces3 belongs to the carboxylesterase family and is enriched in hepatocytes and adipocytes (27). It has been shown to be predominantly in endoplasmic reticulum (ER) (28–30). In this study, we found that in response to cold exposure and β-adrenergic activation, Ces3 targeted LDs and promoted lipolysis. Importantly, we showed that blockage of Ces3 led not only to decreased lipolysis but also to impaired β-adrenergic–stimulated thermogenesis.

RESEARCH DESIGN AND METHODS

Animals

All of the animal studies were reviewed and approved by the Animal Welfare Committee of University of Texas Health Science Center at Houston (animal protocol number AWC-18-0057). Mice were housed in the animal facility (22 ± 1°C) on a 12-h light/dark cycle with ad libitum access to water and regular chow diet, unless indicated otherwise. The Ces3-floxed mouse was a gift from Dr. Richard Lehner at the University of Alberta (Edmonton, Alberta, Canada) (30). Adipose tissue–specific Ces3 heterogeneous knockout (Adn-Cre-Ces3$^{flx/wt}$) mice were generated by crossing adiponectin-Cre with Ces3-floxed mice.

Purification of LD Proteins and Liquid Chromatography–Tandem Mass Spectrometry Analysis

Isolation of LDs was carried out following a previous publication (31). Proteins of LDs were loaded and run on a standard 10% SDS gel. For shotgun proteomics, protein samples were run into resolving gel ~1 cm, and the gel squares containing sample proteins were cut off for analysis. For identification of interest proteins, protein samples were fully separated in SDS-PAGE, and then the gel was stained with the Silver Staining Kit (Thermo Fisher Scientific) following the manufacturer's instructions.

Drug Treatments

Differentiated 3T3-L1 or BAC cells were pretreated with Ces3 inhibitor (WWL229) (10 μmol/L or 100 μmol/L), ATGL inhibitor (atglistatin) (50 μmol/L), PKA inhibitor (PKI 14-22 amide) (10 μmol/L), adenylyl cyclase inhibitor (2′,5′-dideoxyadenosine [ddAdo]) (200 μmol/L), or vehicle separately for 1 h. Then the cells were maintained in the same treatment medium combined with or without 20 μmol/L isoproterenol (ISO) for 6 more hours. Afterward, the cells and cell culture media were harvested for further analysis.

Statistical Analysis

All data were represented as mean ± SEM. Statistical analyses were performed using GraphPad Prism 7 (GraphPad Software Inc). The Student *t* test was applied for statistical significance analysis. A P value <0.05 was considered to be statistically significant.

RESULTS

Identification of Ces3 as a Major LD-Targeting Protein in Mice Challenged by Coldness

To investigate the dynamic changes of the proteins at LD surface, LDs were isolated from the BAT of the cold-exposed mice, and the proteins of LDs were separated by SDS-PAGE (Fig. 1*A*). After silver staining, 12 bands total were found to change, and the proteins in these bands were cut and analyzed by liquid chromatography–tandem mass spectrometry (LC-MS/MS) (Supplementary Fig. 1*A*). Ces3 was the major identified protein of the band highlighted by the arrow (Fig. 1*A*). According to the MS data, 85% of the Ces3 sequences were detected (Supplementary Fig. 1*B*), and an amino acid sequence, LGIWGFFSTGDEHSR, which is specific for Ces3, was identified (Fig. 1*B*). Western blotting (WB) results showed that the samples collected from LDs of BAT in the cold-exposed mice contained a higher level of Ces3 regardless of whether the mice were fed a standard diet (SD) or high-fat diet (HFD) (Fig. 1*C*). Quantitative measurements of the band densities further confirmed the results (Fig. 1*D*). Interestingly, the levels of HSL, phosphorylated HSL (pHSL), as well as perilipin-1 were all increased on the surfaces of LDs upon cold exposure, suggesting the dynamic changes of the LDs (Fig. 1*E*).

In order to compare the proteomic profiles, proteins purified from LDs of the sWAT and BAT in the cold-exposed mice were analyzed by shotgun proteomics. The results showed that among all of those increased proteins upon cold exposure, there are 21 proteins that were increased in both sWAT and BAT (Fig. 1*F*). Heat map data further indicated that in response to cold exposure, more Ces3 were recruited to the LDs in sWAT (Fig. 1*G*). To further verify Ces3 targeting on LDs in sWAT, immunofluorescence (IF) staining with anti-(α-)Ces3 and LD protein perililin-1 was performed on the sWAT from cold-exposed mice. The results showed that compared with the room temperature (RT) condition, there were more yellow signals in the merged images (Fig. 1*H*, red: Ces3; green: perilipin-1), suggesting more LD targeting of Ces3 upon cold exposure. A similar effect was

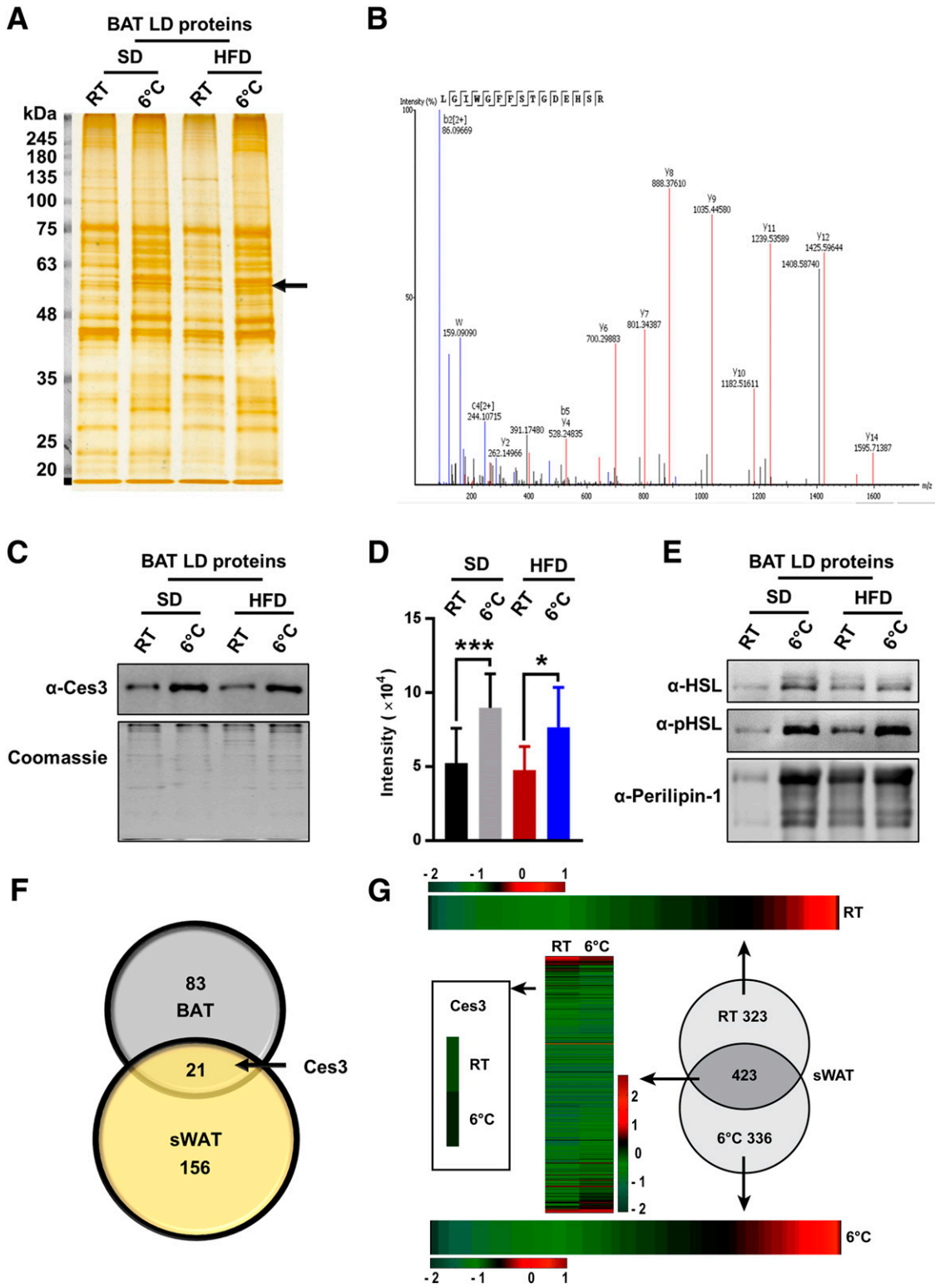

Figure 1—Identification of Ces3 as a major LD-targeting protein in BAT and sWAT of lean and diet-induced obese mice challenged by coldness by LC-MS/MS. *A*: Silver stain of LD proteins isolated from BAT of SD- or HFD-fed mice with or without cold exposure at 6°C (n = 3–6/group). The arrow indicates the band of Ces3. *B*: The mass spectrum of a Ces3-specific amino acid sequence identified from the band indicated by an arrow in *A*. *C*: WB analysis of Ces3 level in the LDs isolated from BAT of the SD- or HFD-fed mice with or without cold exposure at 6°C. The bottom panel is the gel stained by Coomassie blue as loading control. *D*: Quantitative measurement of band density in the WB in *C* (Student t test, $^{*}P < 0.05$; $^{***}P < 0.001$). *E*: WB analysis of the same samples in *C* with α-HSL, α-pHSL (Ser660), and α–perilipin-1 antibodies. *F*: Numbers of LD proteins that increased upon cold exposure in BAT and sWAT. The proteins were obtained from shotgun proteomics. In total, only 83 proteins increased in BAT LDs, only 156 proteins increased in sWAT LDs, and 21 proteins increased in both BAT and sWAT. Ces3 was among these proteins. *G*: Heat maps of LD protein expression level in sWAT of the mice with or without cold exposure at

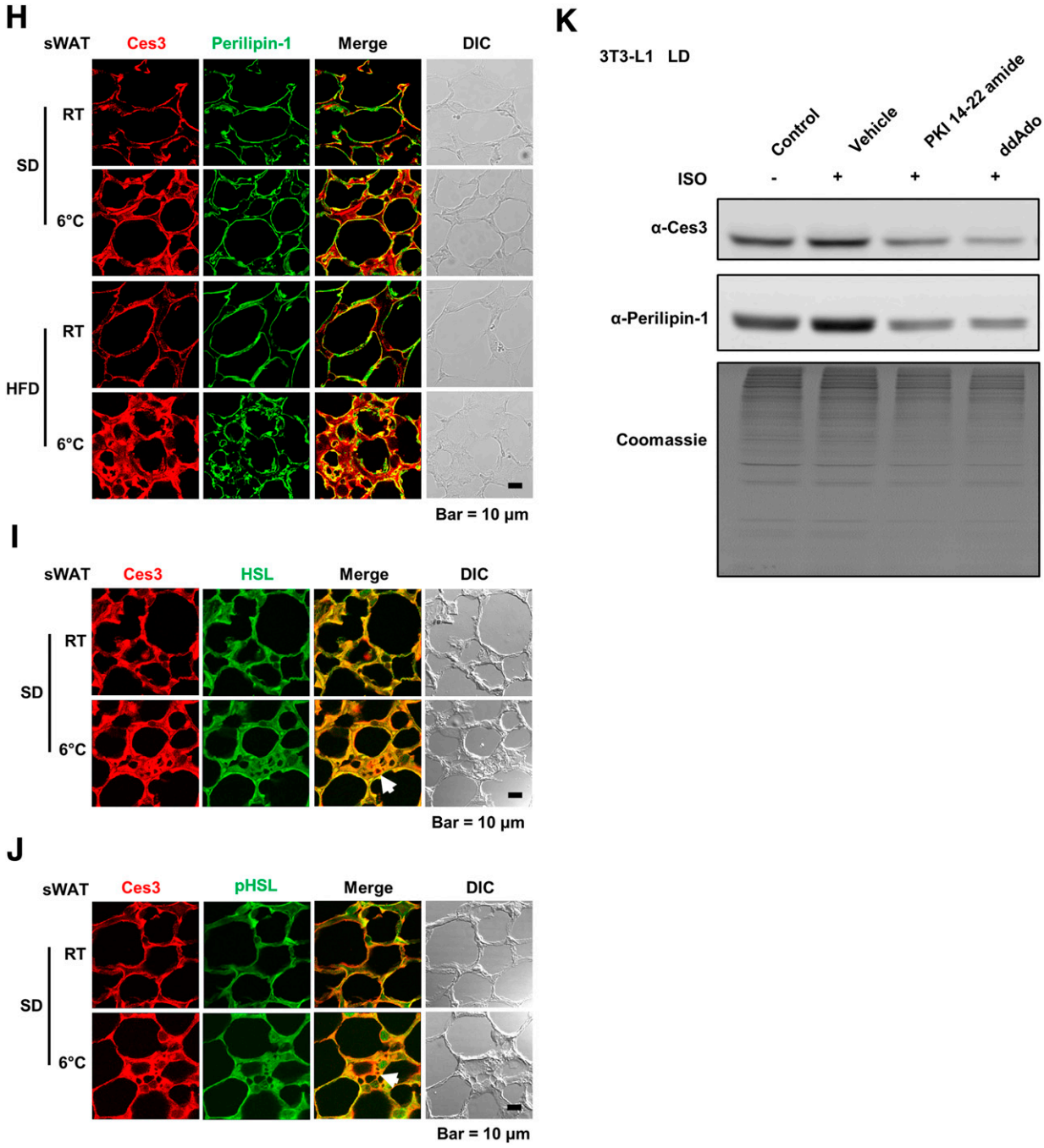

Figure 1—Continued.

observed in the HFD-fed group (Fig. 1*H*, bottom panel). There were also significant amounts of yellow areas in the merged images when Ces3 was costained with HSL or pHSL (Fig. 1*I* and *J*, red: Ces3; green: HSL or pHSL), suggesting cotargeting of Ces3 and HSL in response to cold exposure. Intriguingly, there were regions showing

6°C. Ces3 is highlighted to be increased on LDs from sWAT upon cold exposure. *H*: Co-IF staining with α-Ces3 (red) and α–perilipin-1 (green) antibodies in sWAT of the SD- or HFD-fed mice with or without cold exposure (scale bar, 10 μm). *I*: Co-IF staining with α-Ces3 (red) and α-HSL (green) antibodies in sWAT of the SD-fed mice with or without cold exposure (scale bar, 10 μm). *J*: Co-IF staining with α-Ces3 (red) and α-pHSL (Ser563/565/660) (green) antibodies in sWAT of the SD-fed mice with or without cold exposure (scale bar, 10 μm). *K*: WB analysis of Ces3 level in the LDs isolated from differentiated 3T3-L1 cells treated by ISO together with PKA inhibitor (PKI 14-22 amide; 10 μmol/L) or adenylate cyclase inhibitor (ddAdo; 200 μmol/L). The bottom panel shows the gel stained by Coomassie blue as loading control. DIC, differential interference contrast.

distinct red staining of Ces3, indicating the two lipases were not completely colocalized on LDs (Fig. 1*I* and *J*, arrowheads).

To investigate whether PKA signaling pathways are involved in LD targeting of Ces3, the pharmacological inhibitors were applied. The results indicated that although more Ces3 targeted LDs in response to ISO treatment in differentiated 3T3-L1 cells, cotreatment with PKI 14-22 amide (specific inhibitor of PKA) or ddAdo (specific inhibitor of adenylate cyclase) significantly reduced Ces3 levels on LDs (Fig. 1*K*, top panel). A similar decrease pattern was found for perilipin-1, another LD-targeting protein (Fig. 1*K*, middle panel). These results demonstrated a critical role of PKA-activated pathways in mediating Ces3 translocation onto the LDs.

ISO Treatment Triggers Lipolysis, While the Effect Is Attenuated by Chemical or Genetic Blockade of Ces3

To investigate the function of Ces3 on LDs, WWL229, a Ces3-specific inhibitor, was applied to the differentiated 3T3-L1 and BAC (a brown adipose cell line) cells. The cells were preincubated with BODIPY-C_{12} to stain the LDs and then subjected to ISO treatment. The results showed that upon ISO treatment for 6 h, the BODIPY staining faded more significantly compared with the control group, indicating that the lipolysis process was enhanced in response to ISO (Fig. 2*A*). Expectedly, treatment of atglistatin, an ATGL inhibitor, dramatically blocked the ISO-induced lipolysis effect (Fig. 2*A*, middle panel). Notably, treatment of different doses of WWL229 also had the blocking effect, whereas a higher dose (100 μmol/L) showed a more significant effect (Fig. 2*A*, right panel; quantitative measurement shown in Fig. 2*B*). As the product of lipolysis, glycerol levels in the medium were dramatically decreased upon WWL229 treatment, and the decreased trend showed a dose-dependent manner in response to ISO treatment (Fig. 2*C*). Interestingly, IF staining indicated that upon ISO treatment, more Ces3 colocalized with perilipin-1 (Fig. 2*D*), suggesting more Ces3 targeting LDs. Of note, Ces3 was found to locate distinctly in the niche domains without perilipin-1, and quantitative measurements showed that amounts of Ces3 in the niche domains were significantly increased in response to ISO treatment (Fig. 2*E*, bottom panel shows the quantitative measurement).

The critical role of Ces3 in lipolysis was further verified by a genetic method in vitro. Knockdown of Ces3 with siRNA significantly reduced the glycerol levels upon ISO treatment in both differentiated 3T3-L1 and BAC cells (Fig. 2*F* and *G*) (knockdown efficiency of Ces3 shown in Supplementary Fig. 2). The effect of Ces3 inhibition was further confirmed ex vivo by showing that the glycerol levels in sWAT, epididymal WAT, and BAT were dramatically decreased upon treatment with WWL229 (Fig. 2*H*). The effect was not observed in other tissues, such as liver and muscle (Fig. 2*H*), suggesting the tissue-specific function of WWL229 on lipolytic inhibition.

In summary, both the in vitro and ex vivo results clearly demonstrate that Ces3 plays a critical role in the enhanced lipolysis upon β-adrenergic activation.

Ces3 Does Not Target Autophagosome or Mitochondria in Response to β-Adrenergic Stimulation

LDs and the enzymes on the LDs have been reported to localize in other compartments, including the autophagosome, in the cells (32,33). Protein–protein interaction with LC3, the marker of autophagosome, has been shown to be able to facilitate the autophagosome targeting (32). Because there are multiple LC3-interacting motifs in the Ces3 sequence (Fig. 3*A*), coimmunoprecipitation was performed to test the interaction. The results showed that even though Ces3 molecules were successfully immunoprecipitated with α-GFP antibody, no LC3 was detected by α-LC3 (Fig. 3*B*), suggesting that there is no physical interaction between Ces3 and LC3 under different stimuli. Co-IF with α-Ces3 and α-LC3 in BAC cells further confirmed that Ces3 does not localize into autophagosome upon ISO treatment (Fig. 3*C* [no yellow signal in the merge panels under ISO treatment]).

To detect whether Ces3 targets mitochondria, co-IF staining was performed with α-Ces3 and α-COX IV antibodies (a marker of mitochondria) on the sWAT of the cold-exposed mice. There was no significant yellow signal in the merge image (Fig. 3*D*), suggesting no mitochondrial targeting of Ces3 in response to cold exposure.

To test whether Ces3 trafficked into ER, the 3T3-L1 cells treated with or without ISO were stained with ER tracker (Fig. 3*E*, in green). IF images showed significant amounts of yellow signals (Fig. 3*E*, top and middle panels), suggesting ER localization of Ces3. Interestingly, when all of the nutrients were deprived from the culture medium (Earle's balanced salt solution medium), a similar level of Ces3 targeted into the ER (Fig. 3*E*, bottom panels).

In conclusion, in addition to LDs, Ces3 also targets to the ER. Meanwhile, there is no other compartment localization of Ces3 upon ISO treatment in the adipocytes.

Ces3 Plays an Important Role in the Enhanced Mitochondrial Function Induced by ISO In Vitro and In Vivo

We next demonstrated whether Ces3 affects mitochondrial biogenesis and function. The quantitative PCR (Q-PCR) results showed that the β-oxidation–related genes, including *Acadl*, *Acadm*, *Acads*, *Cpt1a*, *Cpt2*, and *Echs1*, were significantly upregulated in the BAT and sWAT of cold-exposed mice, and WWL229 treatment significantly ameliorated or had the trend to ameliorate the upregulations (Fig. 4*A* and *B*). Intriguingly, the mitochondrial biogenesis-associated genes, such as *Pgc1α*, *Nrf1*, *Cox IV*, and *Tfam*, that were dramatically upregulated by cold exposure were also significantly attenuated

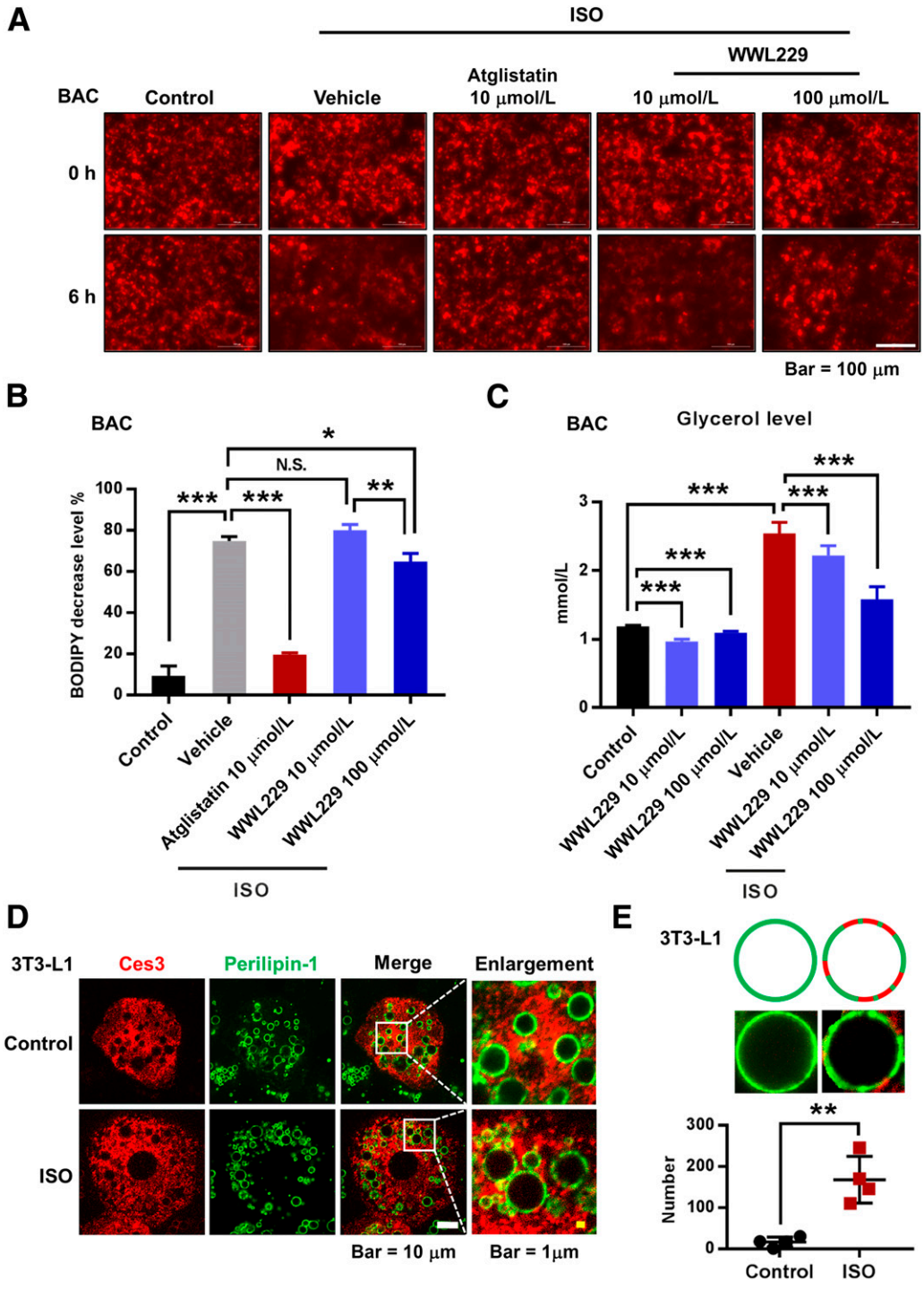

Figure 2—Sympathetic-mimetic ISO treatment triggers lipolysis in differentiated BAC and 3T3-L1 cells, and the effect is attenuated by chemical or genetic blockade of Ces3. *A*: BODIPY staining (for the lipids) of the differentiated BAC cells upon treatments of ISO together with ATGL inhibitor atglistatin or different doses of Ces3 inhibitor WWL229 (scale bar, 100 μm). As the indication of lipolysis, the dynamic fade of BODIPY after 6 h was documented by Cytation 5 imaging reader. *B*: Quantitative measurement of the changes of BODIPY signal in *A* (five fields per group; Student *t* test, $^{*}P < 0.05$; $^{**}P < 0.01$; $^{***}P < 0.001$). *C*: Glycerol level in the culture medium of differentiated BAC cells that were treated with ISO together with or without Ces3 inhibitor WWL229 at different doses (10 μmol/L or 100 μmol/L) (Student *t* test, $^{***}P < 0.001$). *D*: Co-IF staining with α-Ces3 (red) and α–perilipin-1 (green) antibodies in differentiated 3T3-L1 cells treated with or without ISO (left scale bar, 10 μm; right scale bar, 1 μm). *E*: Quantitative measurement of Ces3 (red), which specifically targets LDs but does not colocalize with perilipin-1 (green). The pattern is shown in the top panel. *F*: Glycerol level in the culture medium of differentiated 3T3-L1 cells transfected with scramble or *Ces3* siRNA with or without ISO treatment (Student *t* test, $^{*}P < 0.05$; $^{***}P < 0.001$). *G*: Glycerol level in the culture medium of differentiated BAC cells transfected with scramble or *Ces3* siRNA with or without ISO treatment (Student *t* test, $^{*}P < 0.05$; $^{***}P < 0.001$). *H*: Glycerol level in the ex vivo incubation medium of adipose tissues (sWAT, epididymal WAT [eWAT], and BAT) and nonadipose tissues (liver and muscle) treated with WWL229 and/or ISO (n = 3/group; Student *t* test, $^{*}P < 0.05$; $^{**}P < 0.01$; $^{***}P < 0.001$).

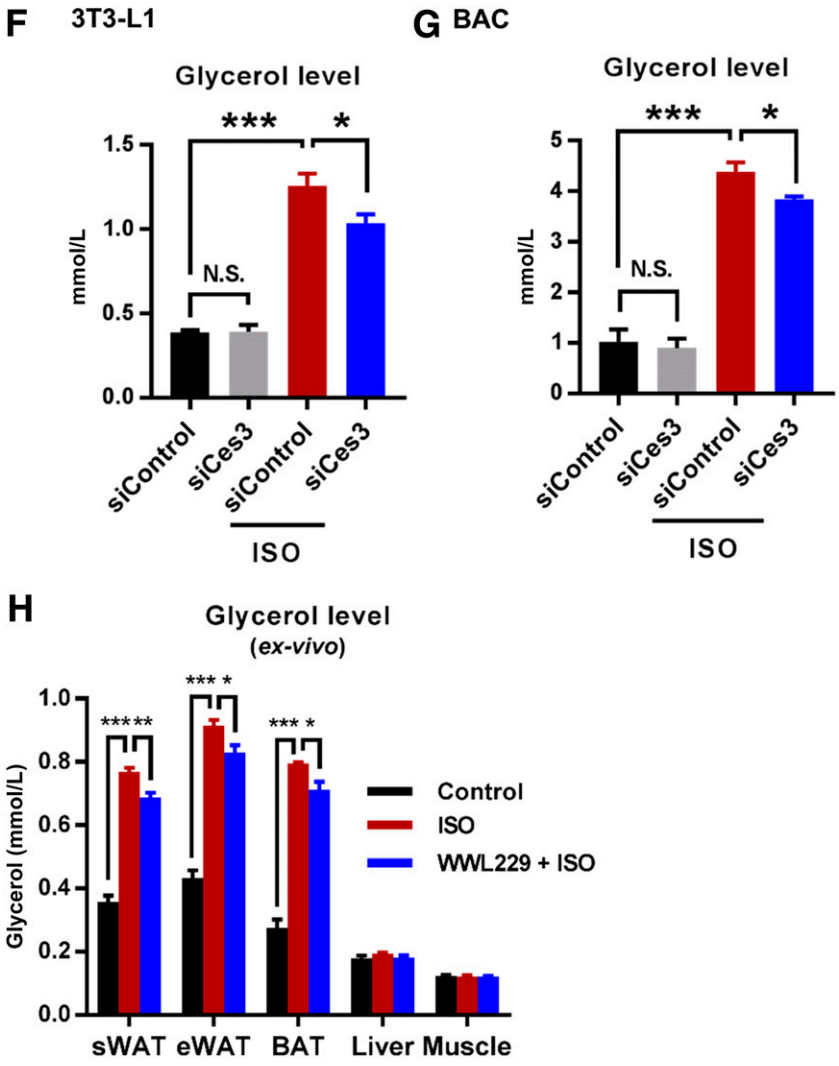

Figure 2—Continued.

or had the trend to be attenuated upon WWL229 treatment (Fig. 4*C* and *D*).

The effects of Ces3 inhibition on mitochondrial function were tested in vitro by chemical and genetic approaches. In the differentiated BAC and 3T3-L1 cells, ISO treatment dramatically upregulated β-oxidation genes, and WWL229 significantly attenuated or had the trend to attenuate the effects (Fig. 4*E* for BAC and data not shown for 3T3-L1 cells). Meanwhile, blockage of Ces3 with siRNA had similar effects on the β-oxidation–related genes (Fig. 4*F*). Of note, the mitochondrial biogenesis-related genes were upregulated by ISO treatment in BAC and 3T3-L1 cells, and the effects were significantly ameliorated by WWL229 (Fig. 4*G* for BAC and data not shown for 3T3-L1 cells). Meanwhile, blockage of Ces3 with siRNA in 3T3-L1 cells had similar effects on these genes (Fig. 4*H*).

To test the effect of Ces3 inhibition on mitochondrial respiration, Seahorse assays were performed on differentiated 3T3-L1 and BAC cells upon Ces3 inhibitions. The results indicated that the oxygen consumption rate (OCR) in differentiated 3T3-L1 cells was significantly reduced upon WWL229 treatment at different time windows during the Seahorse measurement (Fig. 4*I* and *J*). Meanwhile, similar results were observed when blocking Ces3 by siRNA in differentiated 3T3-L1 cells (Fig. 4*K* and *L*). The similar effects of Ces3 inhibition were also observed in BAC cells upon WWL229 treatment (Fig. 4*M* and *N*) and knockdown by siRNA (Fig. 4*O* and *P*).

Ces3 Is Involved in a Sympathetically Activated Thermogenic Program via Activation of PPARγ In Vitro and In Vivo

To determine whether Ces3 is involved in a thermogenic program, WWL229 was applied both in vivo and in vitro. WB indicated that the levels of thermogenic proteins, including UCP1 and PGC1α, were dramatically increased in the BAT of cold-exposed mice, whereas WWL229 treatment significantly attenuated the effect (Fig. 5*A*). Of

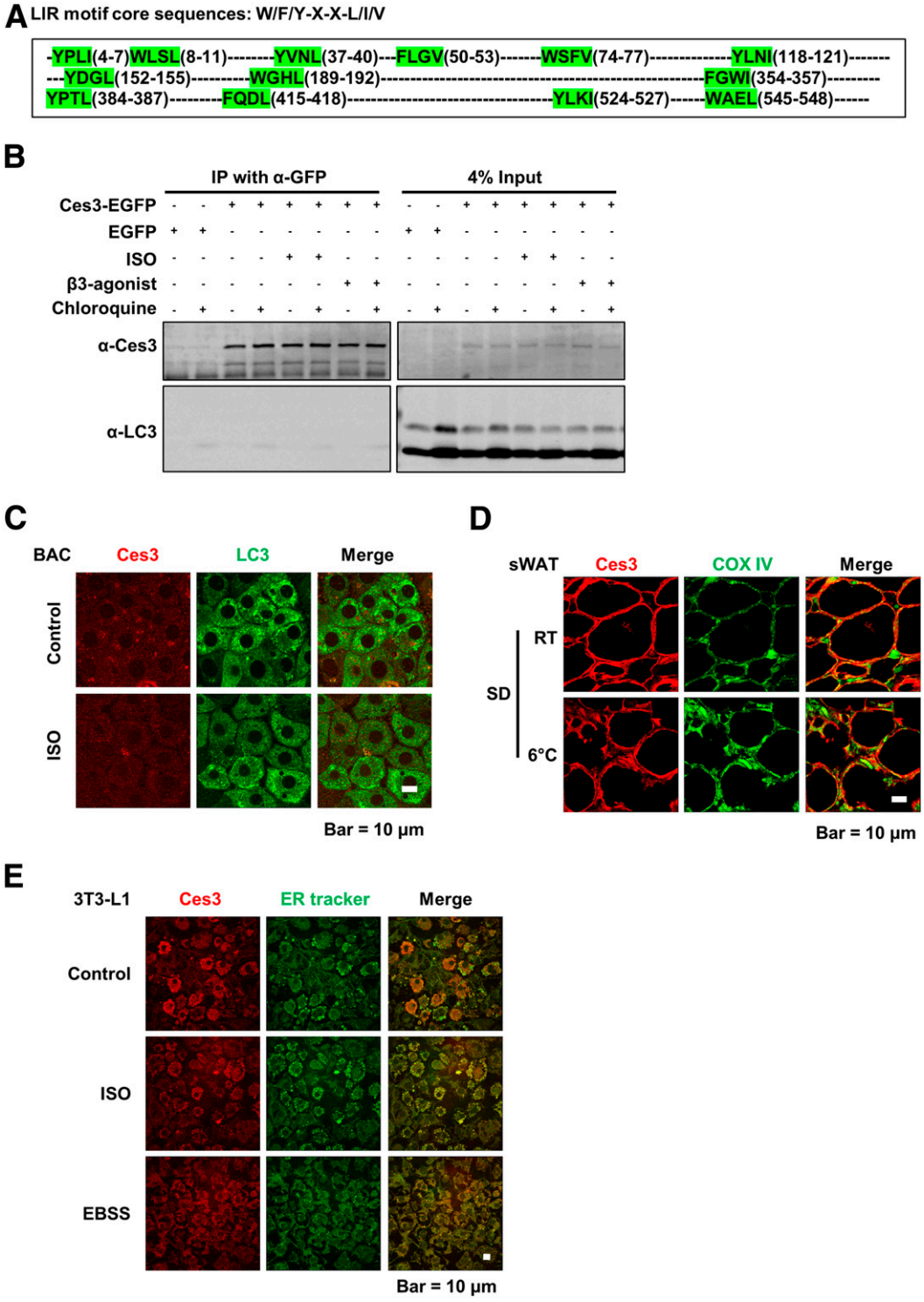

Figure 3—Ces3 targets ER but not autophagosome or mitochondria in response to β-adrenergic stimulation. *A*: The LC3-interacting sequence motif (LIR) is shown at the top, with part of the mouse Ces3 amino acid sequence (UniProt identification number Q8VCT4) shown underneath, which contains 13 LIR motifs total (highlighted by green). *B*: Coimmunoprecipitation (IP) analysis of the interaction between Ces3 and LC3. The cell lysates were IPed with α-GFP antibody followed by immunoblotting with α-Ces3 and α-LC3 antibodies. The lysates were collected from HeLa cells, which were transfected with Ces3-EGFP-pcDNA3 or control EGFP-pcDNA3 and treated with different stimuli, including ISO, β3-agonist, and chloroquine. The right panel indicates 4% input of the cell lysates. *C*: Co-IF staining with α-Ces3 (red) and α-LC3 (green) antibodies in BAC cells upon treatments of ISO (scale bar, 10 μm). *D*: Co-IF staining with α-Ces3 (red) and α-Cox IV (green) antibodies in sWAT of the mice with or without cold exposure (scale bar, 10 μm). *E*: Co-IF imaging with α-Ces3 (red) and ER tracker (green) in differentiated 3T3-L1 cells upon treatments of ISO (middle) or Earle's balanced salt solution medium (EBSS; bottom) (scale bar, 10 μm).

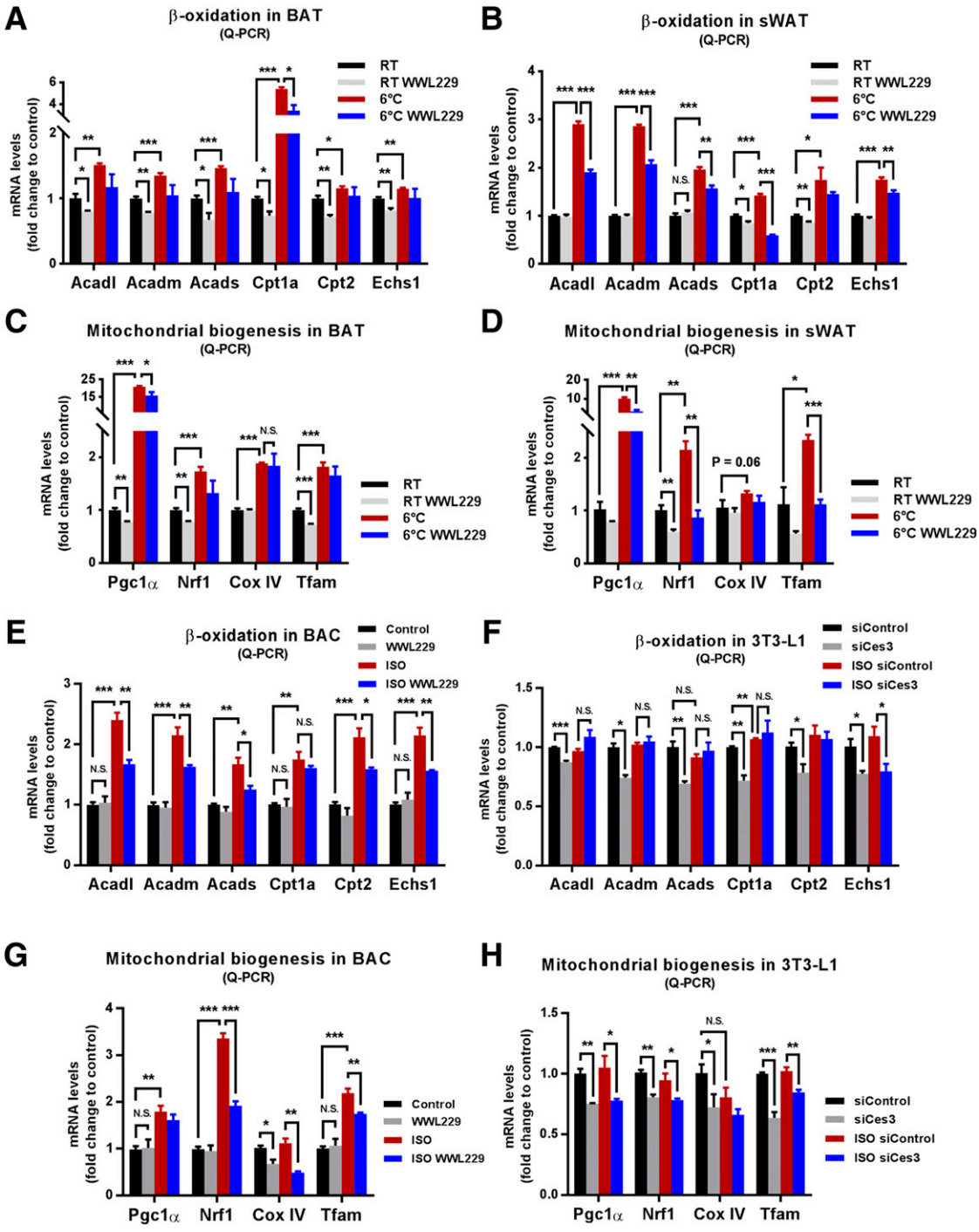

Figure 4—Ces3 plays an important role in the enhanced mitochondrial function induced by ISO in vitro and in vivo. *A*: Q-PCR analysis of β-oxidation genes, namely, *Acadl*, *Acadm*, *Acads*, *Cpt1a*, *Cpt2*, and *Echs1*, in BAT of the mice treated by WWL229 at RT or 6°C (n = 5/group; Student t test, $^*P < 0.05$; $^{**}P < 0.01$; $^{***}P < 0.001$). *B*: Q-PCR analysis of β-oxidation genes, namely, *Acadl*, *Acadm*, *Acads*, *Cpt1a*, *Cpt2*, and *Echs1*, in sWAT of the mice treated by WWL229 at RT or 6°C (n = 5/group; Student t test, $^*P < 0.05$; $^{**}P < 0.01$; $^{***}P < 0.001$). *C*: Q-PCR analysis of mitochondrial biogenetic genes including *Pgc1α*, *Nrf1*, *Cox IV*, and *Tfam* in BAT of the mice treated by WWL229 at RT or 6°C (n = 5/group; Student t test, $^*P < 0.05$; $^{**}P < 0.01$; $^{***}P < 0.001$). *D*: Q-PCR analysis of mitochondrial biogenetic genes including *Pgc1α*, *Nrf1*, *Cox IV*, and *Tfam* genes in sWAT of the mice treated by WWL229 at RT or 6°C (n = 5/group; Student t test, $^*P < 0.05$; $^{**}P < 0.01$; $^{***}P < 0.001$). *E*: Q-PCR analysis of β-oxidation genes, namely, *Acadl*, *Acadm*, *Acads*, *Cpt1a*, *Cpt2*, and *Echs1*, in differentiated BAC cells treated by WWL229 together with or without ISO (n = 5–6/group; Student t test, $^*P < 0.05$; $^{**}P < 0.01$; $^{***}P < 0.001$). *F*: Q-PCR analysis of β-oxidation genes, namely, *Acadl*, *Acadm*, *Acads*, *Cpt1a*, *Cpt2*, and *Echs1*, in differentiated 3T3-L1 cells transfected with scramble or *Ces3* siRNA upon ISO treatment (n = 5/group; Student t test, $^*P < 0.05$; $^{**}P < 0.01$; $^{***}P < 0.001$). *G*: Q-PCR analysis of mitochondrial biogenetic genes including

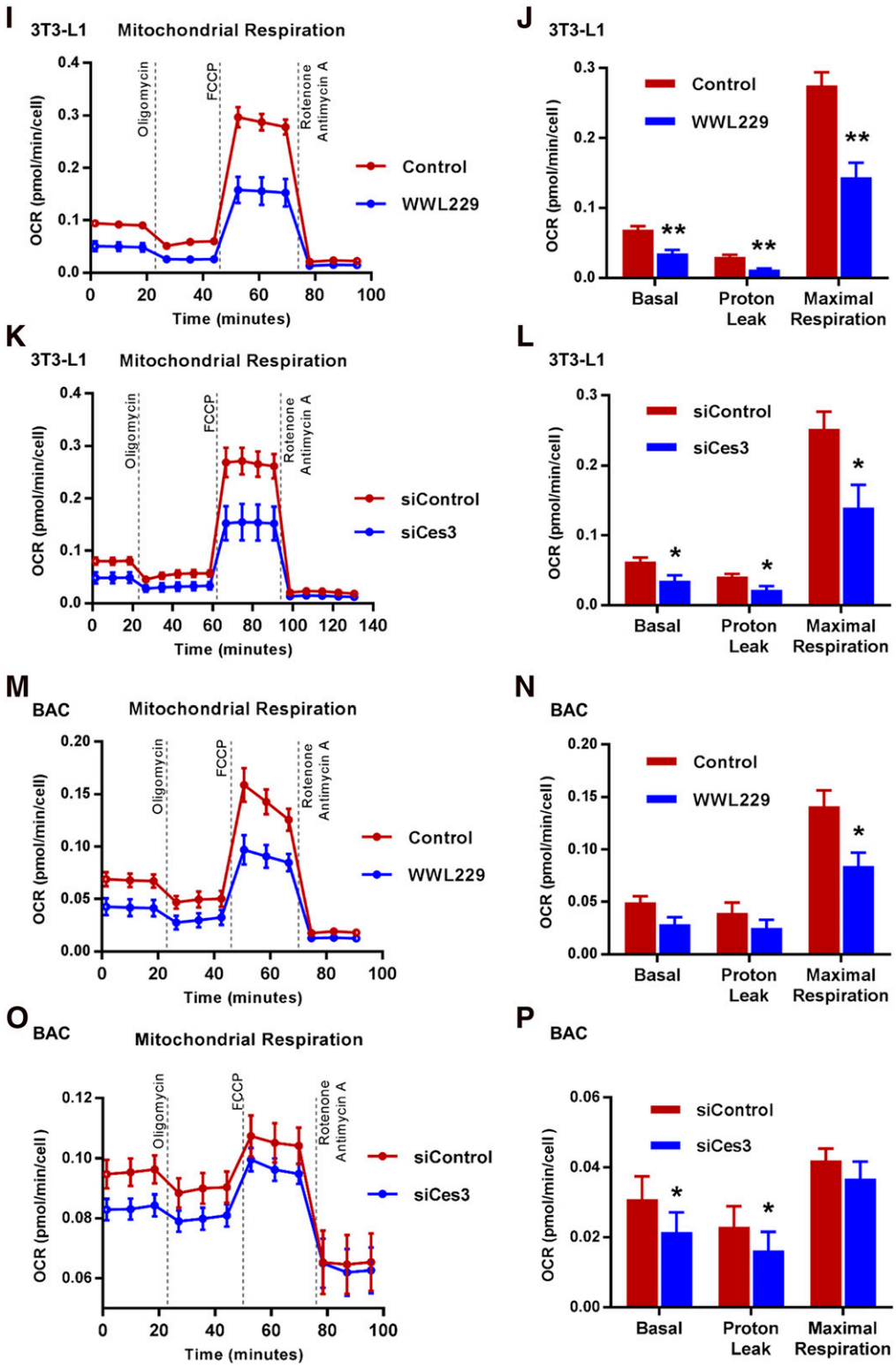

Figure 4—Continued. *Pgc1α*, *Nrf1*, *Cox IV*, and *Tfam* in differentiated BAC cells treated by WWL229 together with or without ISO (n = 5–6/group; Student t test, $^{*}P < 0.05$; $^{**}P < 0.01$; $^{***}P < 0.001$). *H*: Q-PCR analysis of mitochondrial biogenetic genes including *Pgc1α*, *Nrf1*, *Cox IV*, and *Tfam* in differentiated 3T3-L1 cells transfected with scramble or *Ces3* siRNA upon ISO treatment (n = 5/group; Student t test, $^{*}P < 0.05$; $^{**}P < 0.01$; $^{***}P < 0.001$). *I*: The OCR of differentiated 3T3-L1 cells treated with or without WWL229 analyzed by Seahorse instrument (n = 4/group). *J*: Bioenergetic parameters inferred from OCR traces in *I*. Results were represented as mean ± SEM (n = 4/group; Student t test, $^{**}P < 0.01$). *K*: The OCR of differentiated 3T3-L1 cells treated with scramble or *Ces3* siRNA analyzed by Seahorse instrument (n = 4/group). *L*: Bioenergetic parameters inferred from OCR traces in *K*. Results were represented as mean ± SEM (n = 4/group; Student t test, $^{*}P < 0.05$).

interest, the level of CIDE A was also dramatically decreased upon WWL229 treatment, whereas levels of HSL and Ces3 itself did not change (Fig. 5*A*). Notably, mRNA levels of *Ucp1*, *Cide C*, and *Pparγ* were significantly downregulated or had the trend to be downregulated by WWL229 treatment, suggesting the thermogenic regulation by WWL229 is at the level of gene expression (Fig. 5*B*). Similar effects were also observed in the sWAT of the cold-exposed mice (Fig. 5*C* and *D*). Hematoxylin and eosin (H&E) staining further showed fewer multilocular LDs in the sWAT of cold-exposed mice upon WWL229 treatment (Fig. 5*E* and *F*). The IF staining with α-UCP1 antibody verified that the browning effect in sWAT was dramatically impaired by WWL229 (Fig. 5*H*). Of note, because UCP1 maintains at a relatively low expression level at RT, WWL229 treatment did not show a difference for UCP1 in sWAT (Fig. 5*G*).

The thermogenic effect of Ces3 was further confirmed in vitro. Q-PCR analysis showed the downregulation of *Ucp1* and other thermogenic genes upon WWL229 treatment in BAC cells (Fig. 5*I*). Furthermore, UCP1 protein levels were dramatically increased upon ISO treatment, and the effect was significantly attenuated in response to WWL229 treatment (Fig. 5*J*). The WWL229 treatment showed a dose-dependent manner on decrease of UCP1 levels (Supplementary Fig. 3*A* and *B*). Notably, the levels of HSL and Ces3 itself were not affected (Fig. 5*J*, middle panels). Intriguingly, only Ces3 inhibitor, but not ATGL inhibitor (atglistatin), attenuated UCP1 expression (Fig. 5*K*). The Ces3 blockage effects on thermogenesis-associated proteins were further verified by genetic knockdown of *Ces3* in 3T3-L1 cells (Fig. 5*L* and *M*). Of note, genes of other lipases, such as *Atgl*, *Hsl*, and *Mgl*, were not affected by the knockdown of *Ces3* (Supplementary Fig. 4).

We next investigated the mechanisms(s) by which Ces3 upregulates UCP1 in response to β-adrenergic signaling. We found that the serum collected from Ces3 heterozygous knockout mice (Adn-Cre-Ces3$^{flx/wt}$) upon cold exposure failed to increase UCP1 protein levels, whereas the control mice (Ces3$^{flx/wt}$) did (Supplementary Fig. 5, top panel). Moreover, the reduced UCP1 levels caused by Ces3 inhibition were rescued by PPARγ agonist rosiglitazone (Supplementary Fig. 3*C*) in BAC cells. Given that PPARs have been reported to regulate *Ucp1* and other thermogenic genes (11), we then examined the transactivation of PPARα and PPARγ upon activation or inhibition of Ces3. We found that the protein levels of PPARα had no changes in response to Ces3 overexpression or inhibition, whereas PPARγ only slightly decreased when treated by WWL229 or Ces3 siRNA in 3T3-L1 and BAC cells (Supplementary Fig. 6*A–C*) (data not shown for BAC cells). We further performed the luciferase assays by transfecting PPRE for PPARα and PPARγ, respectively, into BAC cells. The results indicate that treatment by WWL229 significantly decreased transcriptional activity of PPARγ/PPARα reporter (Fig. 5*N*), whereas it had no effect on PPARα reporter in response to ISO (Fig. 5*O*, left side shows basal levels were affected by WWL229 treatment). As the demonstration of the Q-PCR results, PPARγ target genes, such as *Glu4*, *Adn*, and *Cd36*, were significantly downregulated by WWL229 in BAC cells (Supplementary Fig. 7). Our results thus suggest that PPARγ-mediated transcriptional regulation plays an important role in Ces3 function on a thermogenic program upon β-adrenergic activation, whereas both PPARα and PPARγ might play a role without β-adrenergic stimulation.

Lipolytic and Thermogenic-Related Factors Are Downregulated in Adipose Tissues of Adn-Cre-Ces3$^{flx/wt}$ Mice

To further investigate Ces3 function in vivo, we generated a conditional knockout line by crossing the floxed Ces3 strain (Ces3$^{flx/flx}$) with the adiponectin-Cre strain (Adn-Cre). The characterization of the double-transgenic line (Adn-Cre-Ces3$^{flx/wt}$) is shown in Supplementary Fig. 8. We used the heterozygous double-transgenic mice to mimic the physiological condition of Ces3 downregulation and the Ces3$^{flx/wt}$ without Cre as the controls. We found that the enhanced lipolysis was significantly ameliorated in the knockout mice when exposed to coldness at 6°C, as indicated by the reduced glycerol production in sWAT and BAT (Fig. 6*A* and *B*). Q-PCR analysis further indicated that *Ucp1* levels were dramatically downregulated in both sWAT and BAT (Fig. 6*C* and *D*). WB and IF results also confirmed that UCP1 protein levels were dramatically decreased in the knockout sWAT and BAT (Fig. 6*E*, *F*, and *H*). The multilocular LD structure also disappeared in the sWAT of the knockout mice (Fig. 6*G*). Of note, we did not observe a significant difference between the knockout and control mice at RT (data not shown). Collectively, knockout of Ces3 specifically in adipose tissue impaired the lipolytic and thermogenic function of the mice when exposed to coldness.

M: The OCR of differentiated BAC cells transfected with or without WWL229 analyzed by Seahorse instrument (n = 4/group). *N*: Bioenergetic parameters inferred from OCR traces in *M*. Results were represented as mean ± SEM (n = 4/group; Student t test, $^*P < 0.05$). *O*: The OCR of differentiated BAC cells treated with scramble or *Ces3* siRNA analyzed by Seahorse instrument. Before Seahorse analysis, the cells were pretreated with ISO for 12 h (n = 5/group). *P*: Bioenergetic parameters inferred from OCR traces in *O*. Results were represented as mean ± SEM. Before Seahorse analysis, the cells were pretreated with ISO for 12 h (n = 5/group; Student t test, $^*P < 0.05$). FCCP, trifluoromethoxy carbonylcyanide phenylhydrazone.

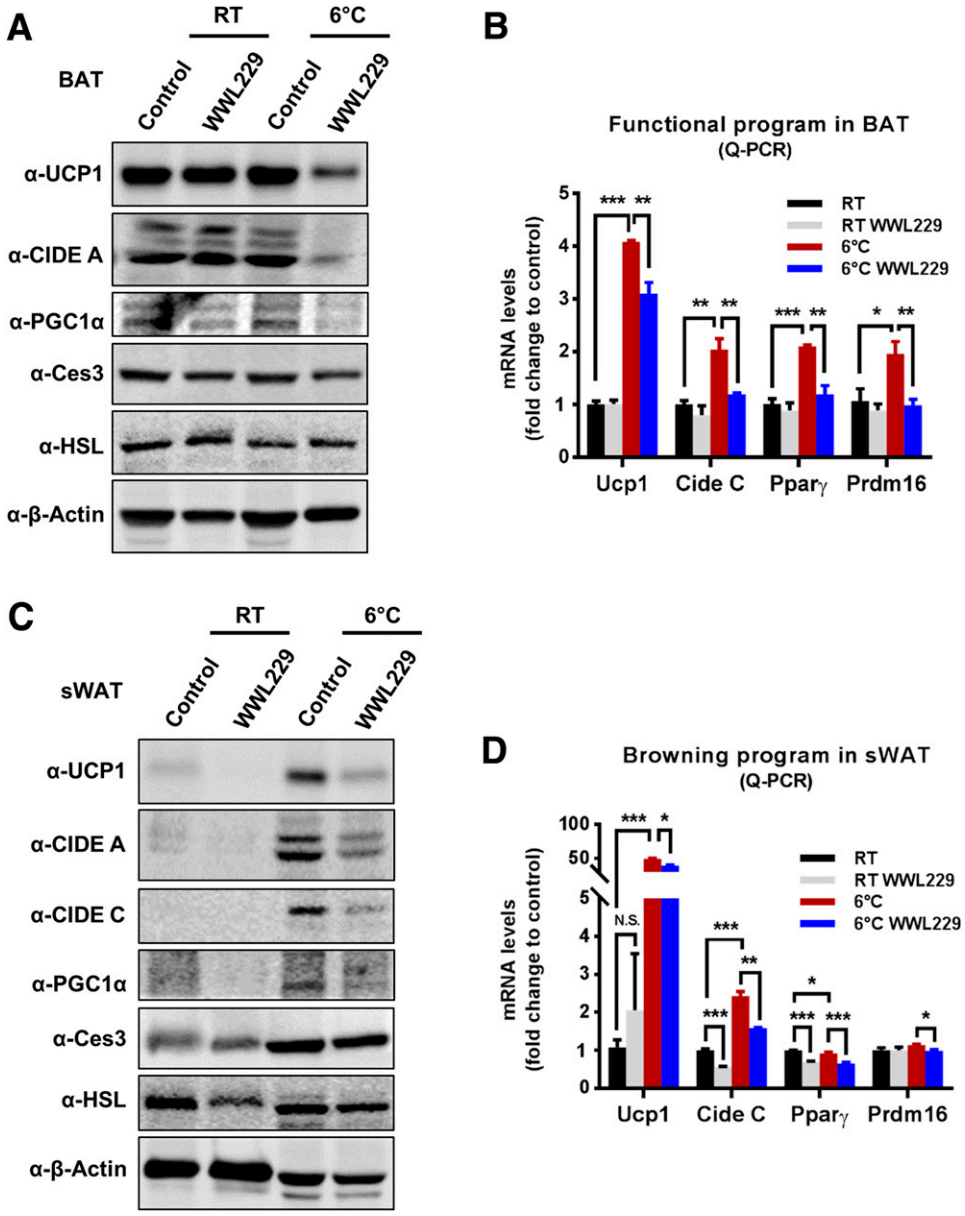

Figure 5— Ces3 is involved in a sympathetically activated thermogenic program via activation of PPARγ in vitro and in vivo. *A*: WB analysis with α-UCP1, α-CIDE A, α-PGC1α, α-Ces3, α-HSL, and α–β-actin antibodies on the whole-cell lysates of BAT collected from the mice treated with or without WWL229 at RT or 6°C (n = 3–5/group). *B*: Q-PCR analysis of functional program genes, including *Ucp1*, *Cide C*, *Pparγ*, and *Prdm16*, in BAT of the mice treated with or without WWL229 at RT 6°C (n = 5–9/group; Student t test, $^*P < 0.05$; $^{**}P < 0.01$; $^{***}P < 0.001$). *C*: WB analysis with α-UCP1, α-CIDE A, α-CIDE C, α-PGC1α, α-Ces3, α-HSL, and α–β-actin antibodies on the whole-cell lysates of sWAT collected from mice treated with or without WWL229 at RT or 6°C (n = 3–5/group). *D*: Q-PCR analysis of browning-related genes, including *Ucp1*, *Cide C*, *Pparγ*, and *Prdm16*, in sWAT of the mice treated with or without WWL229 at RT or 6°C (n = 5–6/group; Student t test, $^*P < 0.05$; $^{**}P < 0.01$; $^{***}P < 0.001$). *E*: H&E staining in sWAT of the mice treated with or without WWL229 at RT (scale bar, 50 μm). *F*: H&E staining in sWAT of the mice treated with or without WWL229 at 6°C (scale bar, 50 μm). *G*: IF staining with α-UCP1 antibody in sWAT of the mice treated with or without WWL229 at RT (scale bar, 10 μm). *H*: IF staining with α-UCP1 antibody in sWAT of the mice treated with or without WWL229 at 6°C (scale bar, 10 μm). *I*: Q-PCR analysis of functional program genes, including *Ucp1*, *Cide C*, *Pparγ*, and *Prdm16*, in differentiated BAC cells treated with ISO together with or without WWL229 (n = 5–6/group; Student t test, $^*P < 0.05$; $^{**}P < 0.01$). *J*: WB analysis with α-UCP1, α-Ces3, α-HSL, and α–β-actin antibodies on cell lysates of the BAC cells treated with ISO together with or without WWL229. *K*: WB analysis with α-UCP1, α-Ces3, and α–β-actin antibodies on cell lysates of BAC cells treated with ISO together with atglistatin or WWL229. *L*: WB analysis with α-Ces3, α-UCP1, α-CIDE A, α-HSL, and α–β-actin antibodies on lysates of 3T3-L1 cells transfected with scramble or *Ces3* siRNA upon ISO treatment. *M*: Q-PCR analysis of browning-related genes, including *Ucp1* and *Cide C*, in differentiated 3T3-L1 cells transfected with scramble or *Ces3* siRNA upon ISO treatment (n = 3/group; Student t test, $^{**}P < 0.01$; $^{***}P < 0.001$). *N*: Analysis of luciferase reporter activity for PPARγ plus PPARα in differentiated BAC cells treated with WWL229 together with or without ISO (n = 3/group; Student t test, $^*P < 0.05$; $^{**}P < 0.01$). *O*: Analysis of luciferase reporter activity for PPARα in differentiated BAC cells treated with WWL229 together with or without ISO (n = 3/group; Student t test, $^*P < 0.05$). RLU, relative light units.

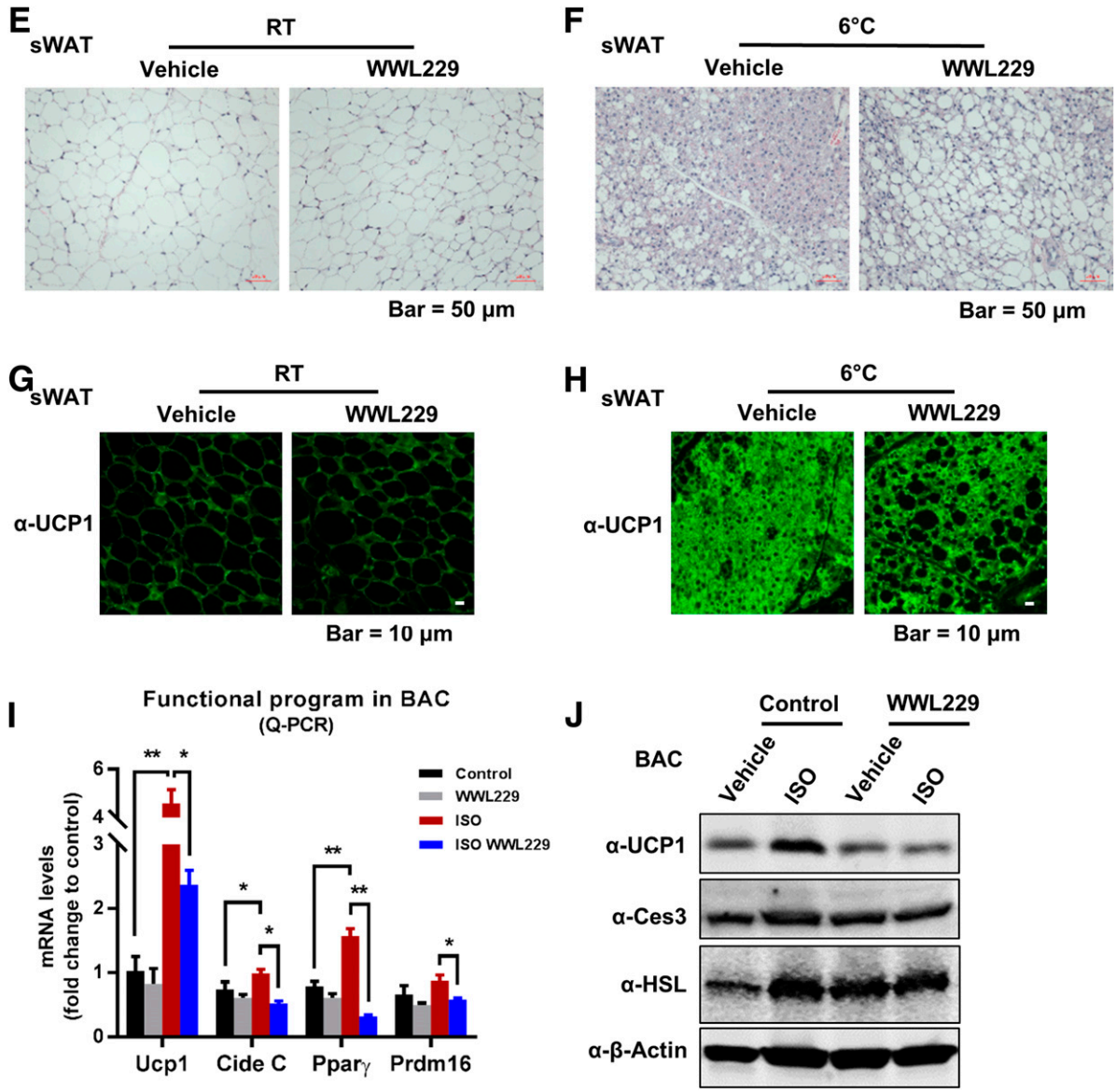

Figure 5—Continued

Blockade of Ces3 by WWL229 or Genetic Knockout Decreases the Ability of Mice to Defend Their Body Temperature When Exposed to Coldness

To investigate the role of Ces3 inhibition on body temperature, the wild-type C57BL/6 mice that were pretreated with or without WWL229 were exposed to coldness at 6°C for 12 h. The results indicated that the WWL229-treated mice exhibited a slight but significant difference when kept at RT (Supplementary Fig. 9*A* and *B*). However, the treated mice showed a dramatically impaired ability to defend their body temperature when kept at coldness (Fig. 7*A* and *B*). Similar results were shown in the Ces3 heterozygous knockout mice (Fig. 7*C* and *D*). Intriguingly, althouogh the impaired thermogenesis was the major effect in the transient cold exposure assay, other energy expenditure–related parameters, such as oxygen consumption and carbon dioxide production, also showed a trend of decrease upon WWL229 treatment (Supplementary Fig. 9*C–F*). Given that UCP-1 is not expressed in sWAT of thermoneutral conditions, we did not perform the test under this condition. In summary, Ces3 inhibition has a dramatic effect on a thermogenic program both in vivo and in vitro.

Taken together, a working model is proposed based on the results (Fig. 7*E*), in which cold exposure and β-adrenergic stimulation trigger Ces3 to translocate into LDs. On the surface of LDs, activated Ces3 digests triglycerides via lipolysis. This lipolytic process might produce unique FFAs that serve as ligands for transcriptional factors, such as PPARs, which in turn upregulate the expression of UCP1 in adipocytes, ultimately leading to an enhanced thermogenic program.

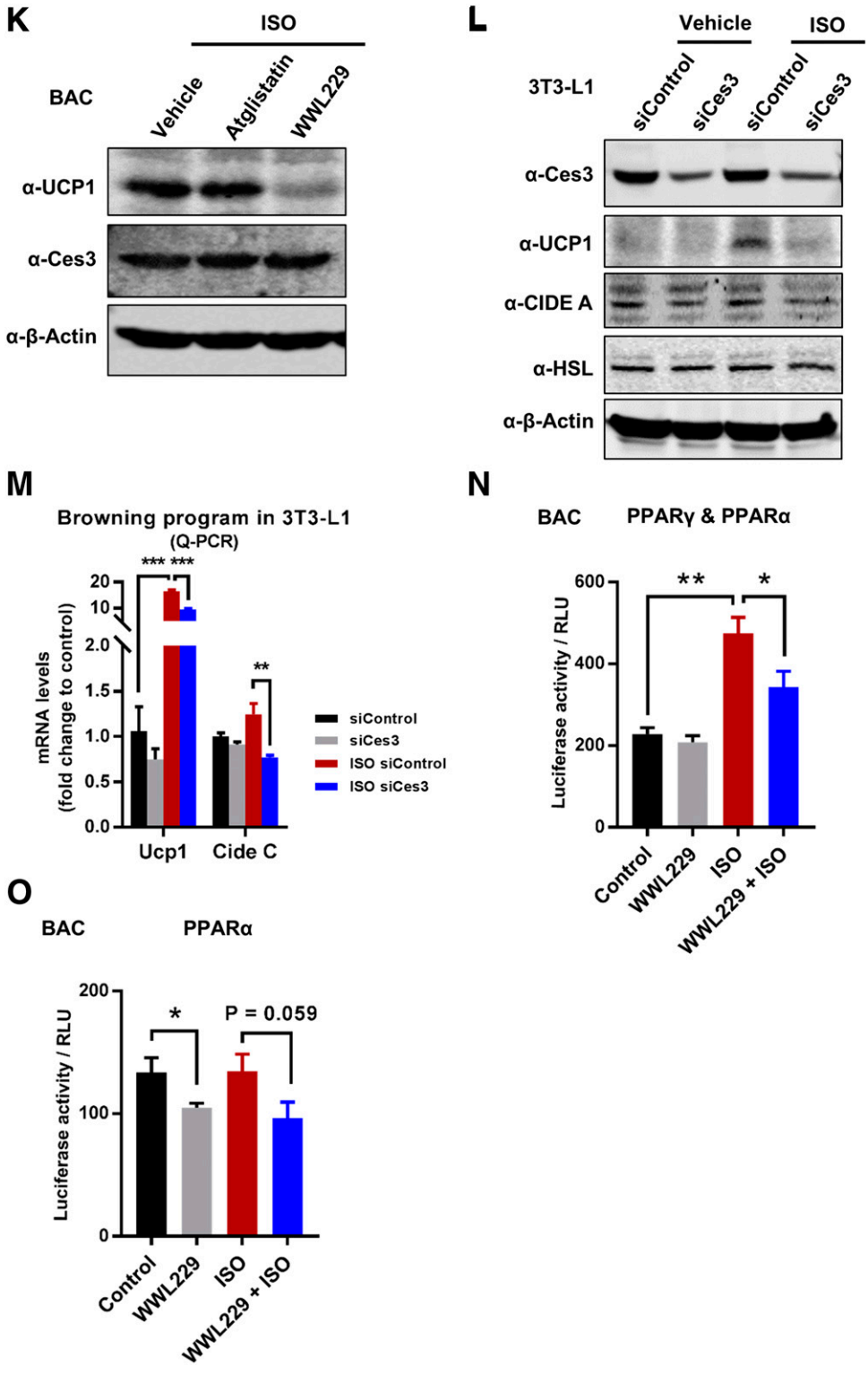

Figure 5—Continued

DISCUSSION

Adipose tissue is the major site to store and burn energy (11). The cytosol LDs are very dynamic in response to divergent energy demands in adipocytes (28,34,35). In response to sympathetic activation, lipolysis is stimulated via a β-adrenergic signaling–triggered cAMP-PKA pathway followed by downstream events, including phosphorylation and activation of lipases such as ATGL, HSL, and monoacylglycerol lipase (36–38). Different species of FFAs are the products of

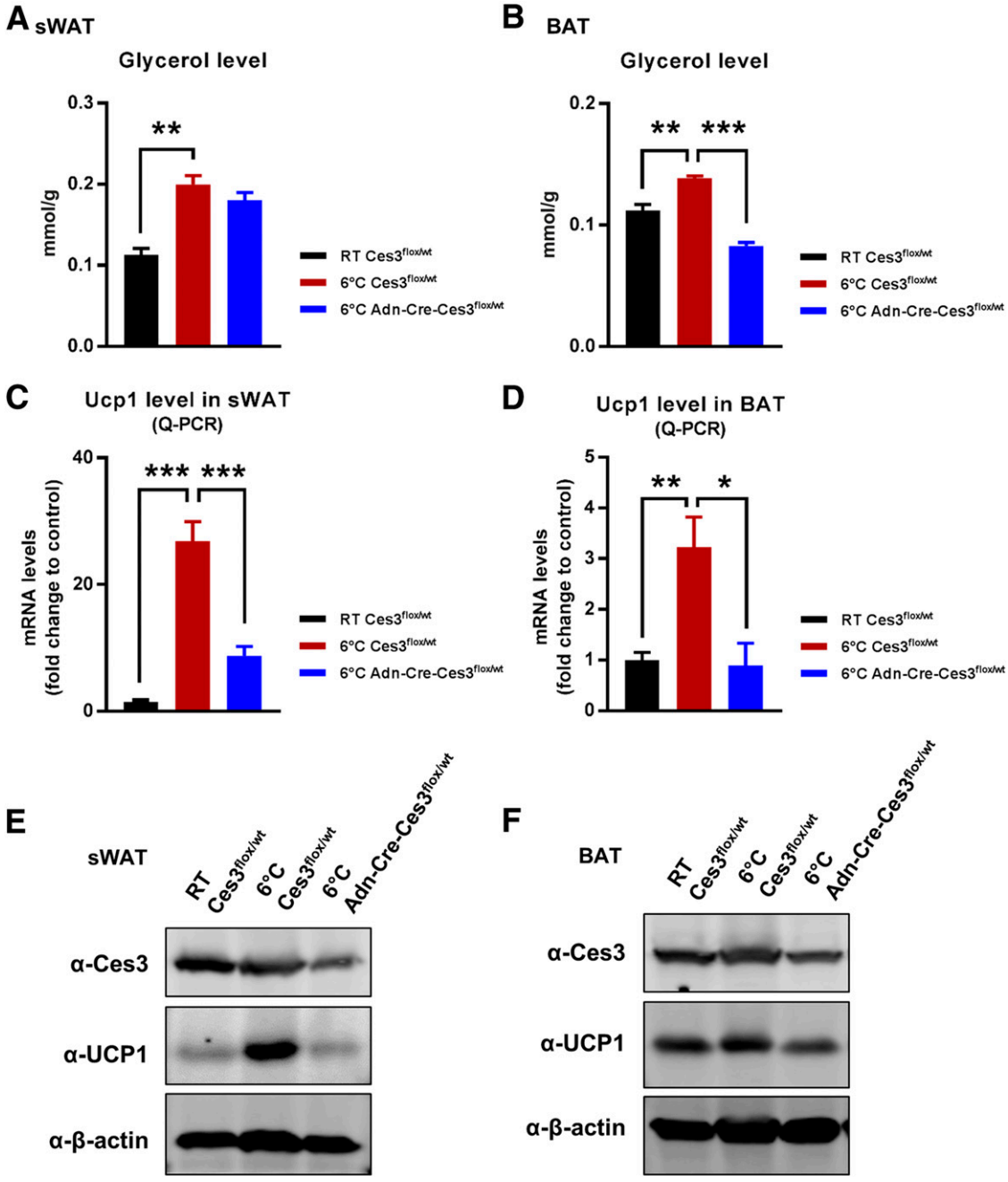

Figure 6— Lipolytic and thermogenic-related factors are downregulated in adipose tissues of Adn-Cre-Ces3$^{flx/wt}$ mice. *A*: Glycerol level in the sWAT of Ces3$^{flx/wt}$ and Adn-Cre-Ces3$^{flx/wt}$ mice at RT or 6°C (n = 3/group; Student t test, $^{**}P < 0.01$). *B*: Glycerol level in the BAT of Ces3$^{flx/wt}$ and Adn-Cre-Ces3$^{flx/wt}$ mice at RT or 6°C (n = 3/group; Student t test, $^{**}P < 0.01$; $^{***}P < 0.001$). *C*: Q-PCR analysis of *Ucp1* level in the sWAT of Ces3$^{flx/wt}$ and Adn-Cre-Ces3$^{flx/wt}$ mice at RT or 6°C (n = 8/group; Student t test, $^{***}P < 0.001$). *D*: Q-PCR analysis of *Ucp1* level in the BAT of Ces3$^{flx/wt}$ and Adn-Cre-Ces3$^{flx/wt}$ mice at RT or 6°C (n = 3–6/group; Student t test, $^{*}P < 0.05$; $^{**}P < 0.01$). *E*: WB analysis with α-Ces3, α-UCP1, and α–β-actin antibodies on lysates of sWAT of Ces3$^{flx/wt}$ and Adn-Cre-Ces3$^{flx/wt}$ mice at RT or 6°C (n = 3/group). *F*: WB analysis with α-Ces3, α-UCP1, and α–β-actin antibodies on lysates of BAT of Ces3$^{flx/wt}$ and Adn-Cre-Ces3$^{flx/wt}$ mice at RT or 6°C (n = 3/group). *G*: H&E staining in sWAT of Ces3$^{flx/wt}$ and Adn-Cre-Ces3$^{flx/wt}$ mice at RT or 6°C (scale bar, 50 μm). *H*: IF staining with α-UCP1 antibody and DAPI in sWAT of Ces3$^{flx/wt}$ and Adn-Cre-Ces3$^{flx/wt}$ mice at RT or 6°C (scale bar, 10 μm).

lipolysis that fuel the thermogenesis and energy expenditure (9). BAT is the predominant organ to burn energy (39). Stimulation of the β3-adrenergic receptor and cold exposure induce a subset of white adipocytes to become "beige" cells, which also accounts for increased thermogenesis and energy expenditure (11,39). Interestingly, recent studies have questioned the role of lipolysis in the thermogenic program in BAT (24,26). In this study, we show that under cold exposure or β3-adrenergic receptor activation, Ces3 targets the cytosol LDs and hydrolyzes

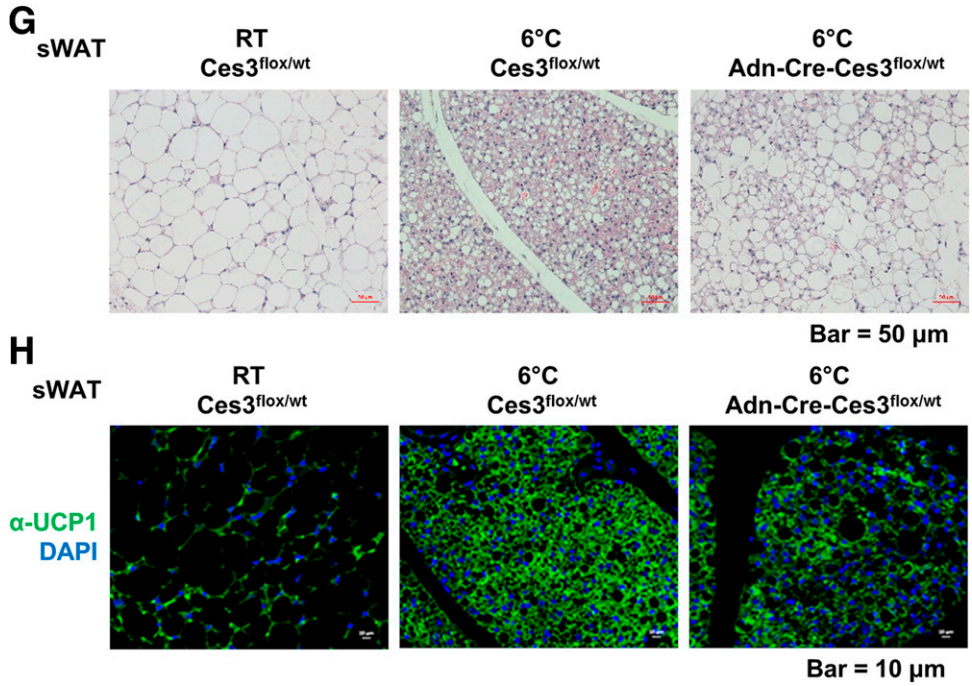

Figure 6—Continued.

the LDs. As the effect, the β-oxidation and oxygen consumption in mitochondria from both WAT and BAT were significantly enhanced. Importantly, we found that β-adrenergic signaling–stimulated upregulation of UCP1 was dramatically attenuated upon Ces3 inhibition. As the result, the WWL229-pretreated or adipose tissue–specific Ces3 knockout mice lost the ability to defend their body temperature under coldness.

We applied WWL229 as the chemical inhibitor for Ces3. Previous reports have demonstrated that WWL229 specifically targets and inhibits Ces3 activity without affecting other enzymes in the family (40,41). Notably, it has also been demonstrated to have no direct function on UCP1 (41). In our study, we confirmed the previous reports of these results. We further demonstrated that WWL229 did not have effects on other lipases, such as HSL and ATGL. Moreover, it did not affect *Ces3* expression on mRNA level, suggesting its inhibitory function is via direct targeting of Ces3 enzyme activity. Of note, even though WWL229 was administrated systemically, its major targets were the adipose tissues upon cold exposure. This tissue-specific effect could be due to more dynamic lipid metabolism in adipose tissues in response to β-adrenergic stimulation. Importantly, all of the effects of WWL229 on adipose tissue were confirmed in adipose tissue–specific Ces3 knockout mice.

In this study, we identified Ces3, which targets LDs in both WAT and BAT in response to cold exposure. We confirmed the LD localization of Ces3 in adipocytes in vitro when triggering the β-adrenergic signaling with ISO. Previously, Ces3 was shown to predominantly locate in the ER lumen to mobilize luminal TG for VLDL synthesis, and its LD targeting is very minor in the adipocytes without treatment (42–44). In this study, we reported that upon cold exposure or β-adrenergic stimulation, Ces3 translocalized to LDs from ER. Interestingly, we found that at the surface of the LDs, even though Ces3 showed colocalization with pHSL and perilipin-1, it also formed some unique spots on LDs without colocalizing with HSL or perilipin-1, suggesting its distinct functions when targeting LDs. Another lipase, ATGL, has been reported to target autophagosome by interacting with LC3 in response to β-adrenergic stimulation (33). Even though Ces3 contains multiple LC3-interacting motifs, it does not physically contact LC3 and target autophagosome under multiple stimuli. Moreover, Ces3 does not target mitochondria in response to different stimuli. Despite no targeting effect, we found that Ces3 inhibition impaired mitochondrial β-oxidation and oxygen consumption both in vivo and in vitro. Moreover, the mitochondrial biogenesis was also adversely affected by the inhibition. These effects might be caused directly by decreased levels of FFAs due to Ces3 inhibition. Because UCP1 is located in the inner membrane of mitochondria, we further hypothesize that downregulation of UCP1 might further lead to abnormal mitochondrial structure and function.

Previously, the link between lipolysis and thermogenesis has been extensively studied. Results from these studies have built a general concept that the lipolysis process provides FFAs that fuel the thermogenesis (9,22). However, more recent studies suggested that lipolysis is not necessary for the heat generation and energy

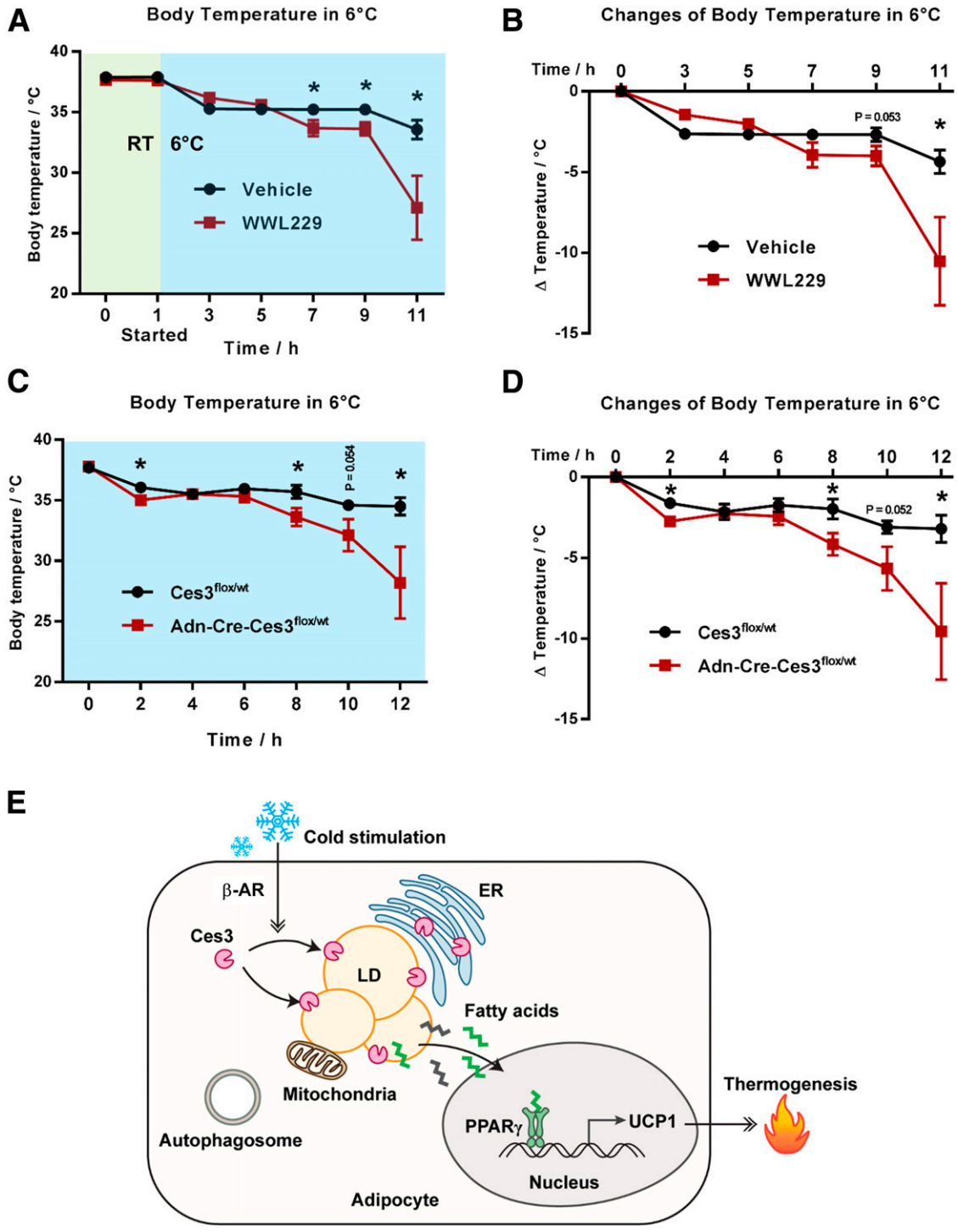

Figure 7—Blockade of Ces3 by WWL229 or genetic knockout decreases the ability of the mice to defend their body temperature when exposed to coldness. *A*: Body temperature of the mice treated with WWL229 at 6°C. The mice were pretreated with WWL229 for 1 h before being transferred into a 6°C room ($n = 6$/group; Student *t* test, $^*P < 0.05$). *B*: Changes of body temperature in *A* compared with time 0 h ($n = 6$/group, Student *t* test, $^*P < 0.05$). *C*: Body temperature of Ces3$^{flx/wt}$ and Adn-Cre-Ces3$^{flx/wt}$ mice at 6°C ($n = 5$/group; Student *t* test, $^*P < 0.05$). *D*: Changes of body temperature in *C* compared with time 0 h ($n = 5$/group; Student *t* test, $^*P < 0.05$). *E*: A proposed working model of Ces3 regulation and function on lipid metabolism in response to β-adrenergic receptor (β-AR) stimulation.

expenditure in BAT (24,26). Of note, these studies were carried out on the in vivo models in which the classic lipolytic molecules were knocked out specifically in BAT (24,26). Thus, the results achieved from these in vivo models might not rule out the possible function of lipolysis via unidentified nonclassical lipid hydrolases on thermogenesis in BAT. In our case, when treating with WWL229 or in the Ces3 knockout mice, the inhibition effect of

lipolysis led to UCP1 downregulation in both WAT and BAT. Moreover, inhibition of Ces3 in 3T3-L1 (white) and BAC (brown) cells had similar effects on UCP1 downregulation. Because UCP1 is the only nonshivering thermogenic molecule, our study suggested lipolysis in both BAT and WAT by Ces3 is linked to the thermogenesis in response to β-adrenergic stimulation. One hypothesis is that lipolysis via Ces3 generates some unique FFAs that serve as ligands to activate specific transcription factors, such as PPARγ, which eventually promote the upregulation of UCP1 genes (refer to the working model in Fig. 7). To support our notion, we found that PPARγ transcriptional activity was downregulated by WWL229 treatment in BAC cells. Moreover, decreased UCP1 expression by Ces3 inhibition can be rescued by a PPARγ ligand named rosiglitazone.

Previously, the adverse effects of Ces3 under the conditions of dyslipidemia and steatohepatitis have been well studied (28–30,45). In the fatty liver, activated Ces3 hydrolyzes lipid contents to produce excessive FFAs as well as assembly VLDL, which in turn causes abnormal accumulation of lipids in liver and other peripheral tissues (28). In that way, blockage of Ces3 function might bring out metabolically beneficial effects, such as decreased circulating lipids, improved glucose tolerance, as well as enhanced energy expenditure (45,46). Of note, these observations do not necessarily contradict our findings given the obviously different metabolic conditions that we investigated. Eventually, we studied the transient activation of Ces3 in adipose tissue in response to sympathetic activation upon cold exposure. Under such short-term physiological stimulation, higher levels of FFAs produced by enhanced lipolysis via Ces3 in adipose tissue do not ectopically circulate to other tissues/organs. Instead, they are used as substrates for accelerated β-oxidation as well as serve as a critical cofactor to activate UCP1 for thermogenesis (19,47). Indeed, we observed an impaired energy expenditure profile when pharmacologically or genetically blocking Ces3.

In conclusion, we have identified Ces3 as a major LD targeting hydrolase in response to cold exposure and β-adrenergic stimulation. Ces3 on the LDs has lipolytic and thermogenic functions. Further studies are warranted to investigate the PKA-mediated pathways that regulate Ces3 translocalization onto LDs and the mechanism(s) by which Ces3 regulates UCP1 expression in adipose tissues. Our findings unveil a previously underappreciated aspect of lipolytic signaling mediated by Ces3, which is particularly essential for energy expenditure, thus highlighting its therapeutic potential to treat obesity and obesity-related metabolic dysregulation.

Acknowledgments. The authors thank Dr. Baharan Fekry and Alexes C. Daquinag at the University of Texas Health Science Center at Houston (Houston, TX) for the technical support, Dr. Zhengmei Mao in the microscopy core of the Brown Foundation Institute of Molecular Medicine for the Prevention of Human Diseases (Houston, TX) for assistance on imaging and tissue processing, as well as Dr. Li Li and Dr. Sheng Pan at the Clinical and Translational Proteomics Service Center at the University of Texas Health Science Center at Houston for the LC-MS/MS analysis. The authors also thank Dr. Yanqiao Zhang at Northeast Ohio Medical University (Rootstown, OH) for the gift of the 3× PPRE-luc (for PPARα) plasmid, Dr. Jiandie Lin at the University of Michigan (Ann Arbor, MI) for the BAC cell line, and Dr. Richard Lehner from the University of Alberta (Edmonton, Alberta, Canada) for the $Ces3^{flx/flx}$ mouse model.

Funding. This study was supported by National Institutes of Health grant R01-DK-109001 (to K.S.) and supported in part by the Clinical and Translational Proteomics Service Center at the University of Texas Health Science Center at Houston.

Duality of Interest. No potential conflicts of interest relevant to this article were reported.

Author Contributions. L.Y. and X.L. performed the experiments, analyzed the data, and assisted with manuscript writing. H.T. and K.Z. contributed to the LC-MS/MS analyses. Z.G. contributed to the research on BAC adipocytes and Seahorse assays. K.S. conceived and designed the research, provided supervision, and wrote the manuscript. K.S. is the guarantor of this work and, as such, had full access to all the data in the study and takes responsibility for the integrity of the data and the accuracy of the data analysis.

References

1. Nielsen TS, Jessen N, Jørgensen JO, Møller N, Lund S. Dissecting adipose tissue lipolysis: molecular regulation and implications for metabolic disease. J Mol Endocrinol 2014;52:R199–R222

2. Xu S, Zhang X, Liu P. Lipid droplet proteins and metabolic diseases. Biochim Biophys Acta Mol Basis Dis 2018;1864:1968–1983

3. Brasaemle DL, Dolios G, Shapiro L, Wang R. Proteomic analysis of proteins associated with lipid droplets of basal and lipolytically stimulated 3T3-L1 adipocytes. J Biol Chem 2004;279:46835–46842

4. Khor VK, Shen WJ, Kraemer FB. Lipid droplet metabolism. Curr Opin Clin Nutr Metab Care 2013;16:632–637

5. Sztalryd C, Brasaemle DL. The perilipin family of lipid droplet proteins: gatekeepers of intracellular lipolysis. Biochim Biophys Acta Mol Cell Biol Lipids 2017;1862:1221–1232

6. Zimmermann R, Strauss JG, Haemmerle G, et al. Fat mobilization in adipose tissue is promoted by adipose triglyceride lipase. Science 2004;306:1383–1386

7. Sztalryd C, Xu G, Dorward H, et al. Perilipin A is essential for the translocation of hormone-sensitive lipase during lipolytic activation. J Cell Biol 2003;161:1093–1103

8. Schweiger M, Schreiber R, Haemmerle G, et al. Adipose triglyceride lipase and hormone-sensitive lipase are the major enzymes in adipose tissue triacylglycerol catabolism. J Biol Chem 2006;281:40236–40241

9. Zechner R, Zimmermann R, Eichmann TO, et al. FAT SIGNALS—lipases and lipolysis in lipid metabolism and signaling. Cell Metab 2012;15:279–291

10. Ahmadian M, Duncan RE, Sul HS. The skinny on fat: lipolysis and fatty acid utilization in adipocytes. Trends Endocrinol Metab 2009;20:424–428

11. Rosen ED, Spiegelman BM. What we talk about when we talk about fat. Cell 2014;156:20–44

12. Nedergaard J, Golozoubova V, Matthias A, Asadi A, Jacobsson A, Cannon B. UCP1: the only protein able to mediate adaptive non-shivering thermogenesis and metabolic inefficiency. Biochim Biophys Acta 2001;1504:82–106

13. Golozoubova V, Hohtola E, Matthias A, Jacobsson A, Cannon B, Nedergaard J. Only UCP1 can mediate adaptive nonshivering thermogenesis in the cold. FASEB J 2001;15:2048–2050

14. Matthias A, Ohlson KB, Fredriksson JM, Jacobsson A, Nedergaard J, Cannon B. Thermogenic responses in brown fat cells are fully UCP1-dependent. UCP2 or UCP3 do not substitute for UCP1 in adrenergically or fatty scid-induced thermogenesis. J Biol Chem 2000;275:25073–25081

15. Harms M, Seale P. Brown and beige fat: development, function and therapeutic potential. Nat Med 2013;19:1252–1263

16. Guerra C, Koza RA, Yamashita H, Walsh K, Kozak LP. Emergence of brown adipocytes in white fat in mice is under genetic control. Effects on body weight and adiposity. J Clin Invest 1998;102:412–420
17. Himms-Hagen J, Melnyk A, Zingaretti MC, Ceresi E, Barbatelli G, Cinti S. Multilocular fat cells in WAT of CL-316243-treated rats derive directly from white adipocytes. Am J Physiol Cell Physiol 2000;279:C670–C681
18. Petrovic N, Walden TB, Shabalina IG, Timmons JA, Cannon B, Nedergaard J. Chronic peroxisome proliferator-activated receptor gamma (PPARgamma) activation of epididymally derived white adipocyte cultures reveals a population of thermogenically competent, UCP1-containing adipocytes molecularly distinct from classic brown adipocytes. J Biol Chem 2010;285:7153–7164
19. Zhao Y, Li X, Yang L, et al. Transient overexpression of VEGF-A in adipose tissue promotes energy expenditure via activation of the sympathetic nervous system. Mol Cell Biol 2018;38(22). pii: e00242-18
20. Lynes MD, Leiria LO, Lundh M, et al. The cold-induced lipokine 12,13-diHOME promotes fatty acid transport into brown adipose tissue. Nat Med 2017;23:631–637
21. Lynes MD, Shamsi F, Sustarsic EG, et al. Cold-activated lipid dynamics in adipose tissue highlights a role for cardiolipin in thermogenic metabolism. Cell Rep 2018;24:781–790
22. Cannon B, Nedergaard J. Brown adipose tissue: function and physiological significance. Physiol Rev 2004;84:277–359
23. Fedorenko A, Lishko PV, Kirichok Y. Mechanism of fatty-acid-dependent UCP1 uncoupling in brown fat mitochondria. Cell 2012;151:400–413
24. Shin H, Ma Y, Chanturiya T, et al. Lipolysis in brown adipocytes is not essential for cold-induced thermogenesis in mice. Cell metab 2017;26:764–777.e5
25. Bråkenhielm E, Cao R, Gao B, et al. Angiogenesis inhibitor, TNP-470, prevents diet-induced and genetic obesity in mice. Circ Res 2004;94:1579–1588
26. Shin H, Shi H, Xue B, Yu L. What activates thermogenesis when lipid droplet lipolysis is absent in brown adipocytes? Adipocyte 2018:1–5
27. Sanghani SP, Quinney SK, Fredenburg TB, Davis WI, Murry DJ, Bosron WF. Hydrolysis of irinotecan and its oxidative metabolites, 7-ethyl-10-[4-N-(5-aminopentanoic acid)-1-piperidino] carbonyloxycamptothecin and 7-ethyl-10-[4-(1-piperidino)-1-amino]-carbonyloxycamptothecin, by human carboxylesterases CES1A1, CES2, and a newly expressed carboxylesterase isoenzyme, CES3. Drug Metab Dispos 2004;32:505–511
28. Lian J, Nelson R, Lehner R. Carboxylesterases in lipid metabolism: from mouse to human. Protein Cell 2018;9:178–195
29. Lian J, Wei E, Wang SP, et al. Liver specific inactivation of carboxylesterase 3/triacylglycerol hydrolase decreases blood lipids without causing severe steatosis in mice. Hepatology 2012;56:2154–2162
30. Lian J, Quiroga AD, Li L, Lehner R. Ces3/TGH deficiency improves dyslipidemia and reduces atherosclerosis in Ldlr(-/-) mice. Circ Res 2012;111:982–990
31. Ding Y, Zhang S, Yang L, et al. Isolating lipid droplets from multiple species. Nat Protoc 2013;8:43–51
32. Birgisdottir AB, Lamark T, Johansen T. The LIR motif - crucial for selective autophagy. J Cell Sci 2013;126:3237–3247
33. Martinez-Lopez N, Garcia-Macia M, Sahu S, et al. Autophagy in the CNS and periphery coordinate lipophagy and lipolysis in the brown adipose tissue and liver. Cell Metab 2016;23:113–127
34. Ducharme NA, Bickel PE. Lipid droplets in lipogenesis and lipolysis. Endocrinology 2008;149:942–949
35. Mottillo EP, Granneman JG. Intracellular fatty acids suppress β-adrenergic induction of PKA-targeted gene expression in white adipocytes. Am J Physiol Endocrinol Metab 2011;301:E122–E131
36. Yehuda-Shnaidman E, Buehrer B, Pi J, Kumar N, Collins S. Acute stimulation of white adipocyte respiration by PKA-induced lipolysis. Diabetes 2010;59:2474–2483
37. Robidoux J, Kumar N, Daniel KW, et al. Maximal beta3-adrenergic regulation of lipolysis involves Src and epidermal growth factor receptor-dependent ERK1/2 activation. J Biol Chem 2006;281:37794–37802
38. He C, Wei Y, Sun K, et al. Beclin 2 functions in autophagy, degradation of G protein-coupled receptors, and metabolism. Cell 2013;154:1085–1099
39. Feldmann HM, Golozoubova V, Cannon B, Nedergaard J. UCP1 ablation induces obesity and abolishes diet-induced thermogenesis in mice exempt from thermal stress by living at thermoneutrality. Cell Metab 2009;9:203–209
40. Dominguez E, Galmozzi A, Chang JW, et al. Integrated phenotypic and activity-based profiling links Ces3 to obesity and diabetes. Nat Chem Biol 2014;10:113–121
41. Galmozzi A, Sonne SB, Altshuler-Keylin S, et al. ThermoMouse: an in vivo model to identify modulators of UCP1 expression in brown adipose tissue. Cell Rep 2014;9:1584–1593
42. Wang H, Gilham D, Lehner R. Proteomic and lipid characterization of apolipoprotein B-free luminal lipid droplets from mouse liver microsomes: implications for very low density lipoprotein assembly. J Biol Chem 2007;282:33218–33226
43. Wang H, Wei E, Quiroga AD, Sun X, Touret N, Lehner R. Altered lipid droplet dynamics in hepatocytes lacking triacylglycerol hydrolase expression. Mol Biol Cell 2010;21:1991–2000
44. Okazaki H, Igarashi M, Nishi M, et al. Identification of a novel member of the carboxylesterase family that hydrolyzes triacylglycerol: a potential role in adipocyte lipolysis. Diabetes 2006;55:2091–2097
45. Lian J, Wei E, Groenendyk J, et al. Ces3/TGH deficiency attenuates steatohepatitis. Sci Rep 2016;6:25747
46. Wei E, Ben Ali Y, Lyon J, et al. Loss of TGH/Ces3 in mice decreases blood lipids, improves glucose tolerance, and increases energy expenditure. Cell Metab 2010;11:183–193
47. Zeng W, Pirzgalska RM, Pereira MM, et al. Sympathetic neuro-adipose connections mediate leptin-driven lipolysis. Cell 2015;163:84–94